## Abstract

This study is focused on the prediction of ice scour loads on a cohesionless seabed in saturated and dry conditions by means of reduced scale physical model testing. The influence of different soil parameters such as the soil permeability and the relative density have been studied in the laboratory under 1g conditions over a range of scouring depths, scouring widths and drifting velocities of an iceberg model. The effect of the drifting speed on the scouring loads was found to be important: a sandy seabed scoured by an iceberg with a mean drifting speed of 0.2 m/s can generate scour loads twice as large as the static loads at prototype scale. The methods used currently to predict ice scour loads consider only the static loads under drained conditions, lower bound, even though some of the methods have been calibrated or compared against experimental results under saturated conditions. In order to calculate the upper bound of the scour loads, the model described in this paper is proposed, which takes into account the undrained (or partly-undrained) responds of a sandy seabed.


## Introduction

Marine structures such as subsea pipelines are at risk of being damaged by deep iceberg-keels. The ice scour process begins when a floating ice mass with a deep keel is driven into shallow water by environmental forces such as winds, water currents and waves. After contact with the seabed, the ice continues to scour until the initial kinetic energy and the work done by driving forces is dissipated through the work done on the seabed, or until the soil resistance exceeds the strength of the ice keel. In this latter scenario, the ice feature can continue to scour the seabed but it is likely that the part of the ice feature in contact with the seabed will experience substantial modifications in shape (Woodworth-Lynas et al., 1991), a process also known as keel degradation. In either case, the scouring loads have to be determined and the accuracy of the model chosen to predict the maximum scouring depth will be dictated, partly, by the accuracy of the predicted scouring loads. An ice feature also has the ability to pitch and heave as indicated in Figure 1. It is also known that during the movement of an iceberg, the soil below will displace horizontally and vertically, a process known as sub-gouge deformation, as reported previously by Been et al. (1990) (Figure 1).

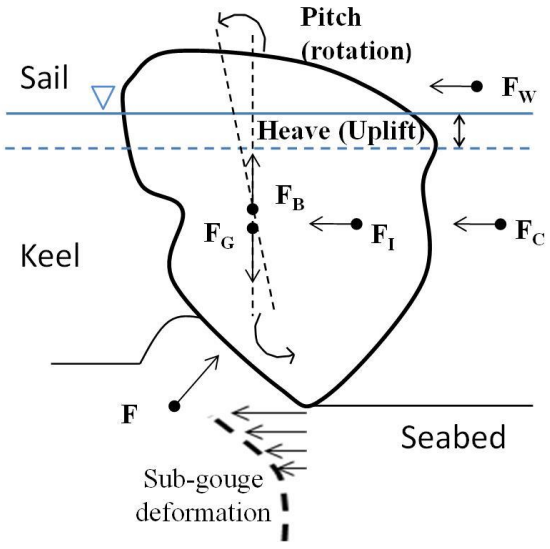


**Figure 1.** General schematic representation of the ice gouging process. $F_W$: wind, $F_C$: water current, F: seabed resistance, $F_G$: weight, $F_B$: ice buoyancy, $F_i$: inertial force.

Barrette and Sudom (2012) compiled a database which consists of 487 physical scour simulations from 28 different studies. General information about the test facility, soil and keel type, test conditions and results are outlined. The database can be utilized to determine if and how any given parameter has been addressed in previous studies, and whether a knowledge gap exist. For example, the keel displacement rate, or drifting speed, has received little attention in the past. In the recent years, an important contribution towards improving the understanding of the ice gouging process and the interaction with the seabed and subsea structures has been made in the recent years (e.g. Been et al., 2013; Eltaher, 2014; Liferov et al., 2014; Paulin et al., 2014). For example, Paulin et al. (2014) discuss the issues and challenges surrounding pipeline trenching and burial in ice gouge environments. It is highlighted that for areas that experience relatively deep ice gouging depths (up to 5 m), burial depth requirements will exceed the capability of current pipeline burial technologies. Been et al. (2013) presented a design process for buried pipelines in ice scour environments and Liferov et al. (2014) developed a numerical model to assess the pipeline response to ice gouging. In this latter study, the importance of the geotechnical conditions and the rake angle, obtaining deeper gouges with steeper rake angles or weaker soils was discussed.

An overall perspective of ice-gouging issues is discussed elsewhere e.g., King (2011), Barrete (2011). A number of physical modelling studies have been undertaken to investigate the ice scour process either through small scale (e.g. Arnau and Ivanovic, 2015; Kioka et al., 2000; Abdelnour and Graham, 1984; Barker and Timco, 2002), large scale (e.g. Peek et al., 2013; Liferov and Høyland, 2004) or centrifuge tests (e.g. Yang, 2009; Hynes, 1998; Allersma and Schoonbeek, 2005; Phillips et al., 2005). A number of ice scour analytical models exist in the literature which attempt to explain the resistance forces associated with the movement of the iceberg while in contact with the seabed. These analytical models are used later to obtain a gouge depth distribution based on the strength of the iceberg keel, energy dissipation, iceberg geometry and soil properties; the most common models referenced are those developed by Been et al. (1990), PRISE model (Walter et al., 1998) and Croasdale et al. (2005), where the scouring event is treated as occurring before undrained conditions.

## Background

### Current methods for scouring load prediction

The theory of kinematic boundary wedges described by Hettiaratchi and Reece (1975) has been implemented by other researchers to estimate the ice scour loads in drained conditions (e.g. Been et al., 1990b; Walter et al., 1998; Croasdale et al., 2005). All these models treat the ice scouring process as a drained event, even though the mean drifting speed of several icebergs around Grand Banks was found to be 0.22 m/s (Smith and Donaldson, 1987) which in combination with a low permeability seabed can develop undrained or party-undrained scouring conditions. The same methodology described by Hettiaratchi and Reece (1975) was used in the present study to calculate the scour loads in dry sand ($F_{static}$) and a detailed explanation of how to compute $F_{static}$ for a range of iceberg geometries and soil properties can be found in Arnau and Ivanovic (2015) and Arnau (2017). Figure 2 shows the geometry of the soil failure mechanism created in front of an iceberg model with the frontal face inclined at an angle $\alpha$ = 150˚, for example. As can be observed, a kinematic wedge is represented in front of the frontal face of the model and a perfectly rough interface (line AB in Figure 2) is created

with a rake angle of (90˚-$\varphi_{crit}$) as described by Hettiaratchi and Reece (1975). From this type of soil failure mechanism with kinematic wedges it is concluded that the basal shear component, the frictional force $F_2$ generated at the base of the kinematic wedge in Figure 2, is the main contributor of the scour load in dry sand.

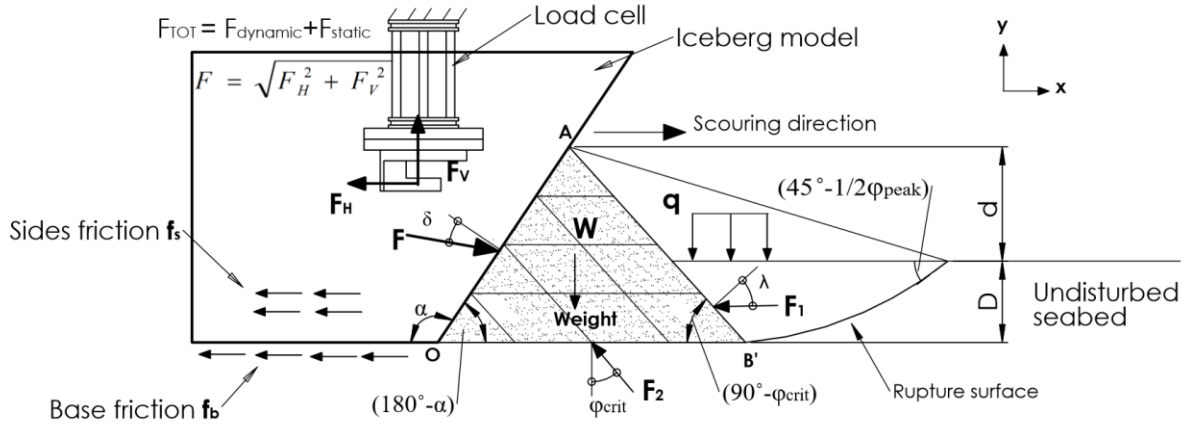


**Figure 2.** Schematic Diagram of the iceberg soil model with the signs and conventions used in this present study. D: scour depth, d: height of sand accumulated in front of the model, B: scour width, α: rake angle, W: kinematic wedge, λ: soil-soil friction angle, $\varphi_{crit}$: critical state friction angle, φ or $\varphi_{peak}$: peak sand friction angle, δ: wall friction angle, q: surcharge, $F_1$: passive earth resistance, $F_2$: reaction force at the base of the kinematic wedge, F: scour load, which can be $F_{TOT}$, $F_{static}$ or $F_{dynamic}$, $F_H$: horizontal scour load, $F_V$: vertical scour load, $f_s$: friction force on the side walls of the iceberg model, $f_b$: friction force on the base of the iceberg model.

Barker and Timco (2002,2003) provided empirical equations to estimate the scour loads from small scale laboratory tests under 1g conditions. Multiple linear regression analysis from laboratory results were performed in order to gain further insight into the dependence of the measured force on the iceberg velocity *v*, scouring depth *D* and scour width *B*. The regression analysis yielded the following relationship represented in eq. [1], where the scour load *F* in kN is a function of the scour depth *D* in meters, scour width *B* in meters and the iceberg velocity *v* in m/s. Although Eq. 1 provides some insight into the measured force's dependence on some iceberg parameters, it does not provide any link or relation to geotechnical aspects such the soil friction angle or what aspects and soil properties control the rate effects (the increase of scour loads with velocity). Note that an aspect ratio (scour width divided by scour depth) of 2 or below was used in this study. Such low values of aspect ratios are difficult to find in real ice scour scenarios. For example King et al. (2009) or the Grand Banks Scour Catalogue (Campbell et al. 2014) report that in which most of the aspect ratios fall within the range of $5 < \frac{B}{D} < 300$.

$$F = 8.5v + 46.3D + 28.5B - 7.6 \quad (1)$$

Kioka et al. (2000) performed a set of scouring tests with rigid indentors (similar to Figure 3) of varying rake angle to calibrate a mechanical scour model. The test were performed in saturated sand and with a seabed slope of 1/50 (1.15°). The drifting speed was varied from 0.01 m/s to 0.2 m/s. Kioka et al. (2000) observed that for drifting speeds ranging from 0 to 0.05 m/s, the scour loads were practically constant. However, the scour loads markedly increased when the drifting speed exceeded 0.05 m/s. It was concluded that the increase of the scour load with drifting speed was mainly due to: an increase

of effective stresses caused by a reduction of the pore water pressure; and an increase of the sand accumulated in front of the iceberg model. The mechanical scour model developed by Kioka et al. (2000) was not able to accurately reproduce the scouring loads when the speed was increased above 0.05 m/s.

Abdelnour and Graham (1984) reported on a series of scour tests in which the drifting speed was also varied and its effect on the scour loads analysed. Three different soils were tested: sand, a sandy silt and a silty clay and the greatest impact was observed in sand, where the measured scour loads increased by 110% as the drifting speed varied from 0.006 m/s to 0.088 m/s.

The increase of scour loads with velocity (rate effects) occurs because the process of sand shearing is accompanied by a tendency for the particles of sand to move apart and consequently for the void space between particles to increase. The increased void space is filled by additional pore water. The pore fluid flows from the surrounding soil governed by a pressure gradient which increases the effective stresses in the soil (Palmer 1999). The work carried out by Lauder et al. (2012) and Lauder and Brown (2014), based on the previous work conducted by Cathie (2001) and Cathie and Wintgens (2001) on the performance of pipeline ploughs, will be used as a basis to analyse the rate effects during ice scouring (see eq. [2]). Kinematic wedges are not developed in the soil failure mechanism during ploughing, for this reason, it is thought that the constant C in eq. [2] will differ from that found by Lauder and Brown (2014). The present study will be focused on changing the geometry of the object being dragged (rake angle α, scour depth D, scour width B) rather than testing with different soils, which was the focus of Lauder et al. (2012).

$$\left(\frac{F_{TOT}}{F_{v=0}} - 1\right) = C \times \frac{vDS}{C_v} \tag{2}$$

where $F_{TOT}$ is the total measured scour load in saturated conditions; $D$ is the scour depth (associated with the drainage path length); $v$ is the velocity of the object penetrating the soil; S is the dilation potential defined as $\Delta e/(1+e_0)$ (where $e_0$ is the initial void ratio and $\Delta e$ is the void ratio increase from initial conditions to $e_{crit}$ ); $C_V$ can be calculated with eq. [3] as reported by Finnie (1993) or Haigh et al. (2012); and $C$ is a constant and is assumed to be a function of the geometry of the object penetrating the soil.

$$C_V = \frac{E_0 k}{\gamma_w} \tag{3}$$

$E_0$ is the one-dimensional stiffness modulus; $k$ is the soil permeability; $\gamma_w$ is the unit weight of water.

Lauder et al. (2012) found that for values of $(vDS/C_V) < 0.0001$ the rate effects are negligible. In a similar way, the dimensionless number $(vDS/C_V)$ can be used to check whether an iceberg scouring a cohesionless seabed with a certain drifting speed will induce any rate effects. Based upon the findings presented later in this paper, a quick estimation indicates that $(vS(D+d)/C_V) > 0.0001$ will generate undrained or party-undrained conditions, which is true for most of the real scour scenarios in a sandy seabed with permeability coefficients lower than $k < 1 \cdot 10^{-3}$ m/s. This reaffirms the need of considering the rate effects during ice scouring. However, none of the force scour models found in the literature capture the rate effects accurately. Thus, this study will attempt to incorporate the influence of the

drifting speed of an iceberg in a force scour model for a range of soil parameters and iceberg geometries.

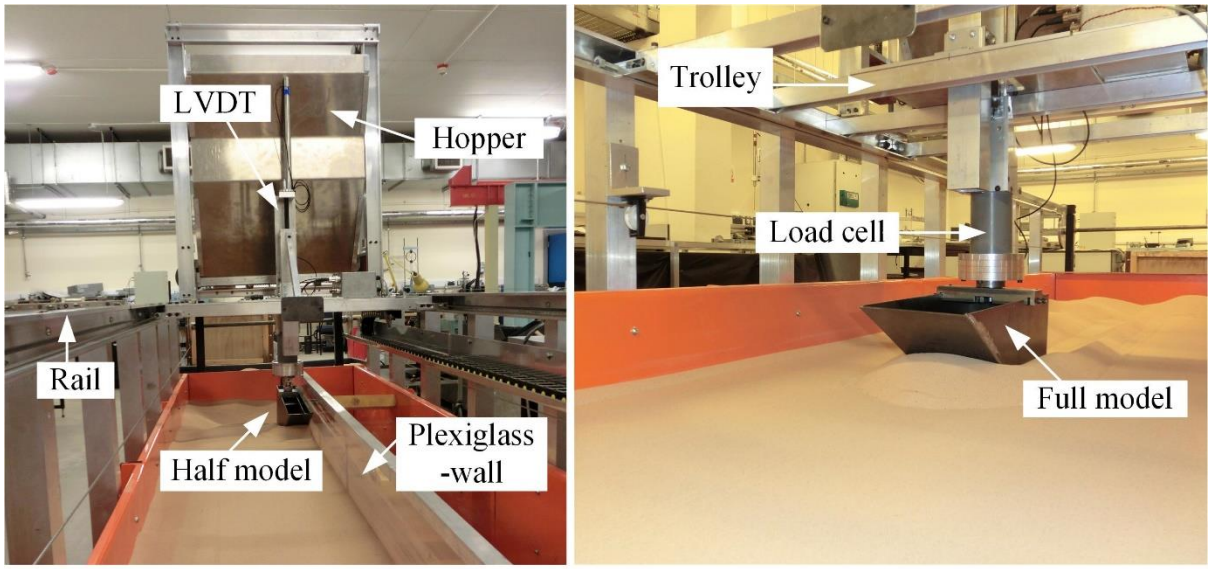


**Figure 3.** Facility for ice scouring tests. (a) Half model and PIV set-up. (b) Full model set-up.

## Experimental setup

Scaled models of an iceberg keel were tested in a 4.8 m long, 0.8 m wide and 0.3 m deep sand channel, based within the University of Aberdeen, and the scour loads (also scour force) and the associated soil disturbance measured (Figure 3). A fine siliceous sand (HST95) was utilized to carry out the tests under both saturated conditions and dry sand and a summary of the physical properties is found in Table 1. This sand is the same utilized by Lauder et al. (2012) and it also very similar to the sand utilized during the PRISE studies (e.g. Hynes, 1996; Winsor and Parson, 1997; Phillips et al., 2005), which will allow the comparison of the results with this present study. Unlike tests in 1g conditions, centrifuge model tests can be performed on undisturbed soil samples, if the effective stress conditions in the sample are representative of the prototype. Macro-fabric present in the undisturbed model sample, such as structure, fissures, inclusions and potential drainage paths, may not scale to be representative of the conditions in the prototype (Phillips, 1995). In order to study the scalability of the results obtained in the present study, three model scales (e.g. different scour width) were tested in 1g conditions.

Scaled iceberg models were pushed along the full channel width (Figure 3b). As described by Barrete and Sudom (2012), two possible set-ups can be used to simulate an ice scouring test in the laboratory: keel heaving prevented (pre-set scour depth) or keel heaving allowed. For this study the former was used. It was assumed that the heave (upward movement) of an iceberg during gouging would be small compared to that of an ice ridge due to the large weight (Mt) of an iceberg. In a real gouging scenario, a small part of the iceberg's weight will be transferred to the soil through the base of the kinematic wedge created in front of the keel. Sand 'pluviation' was used before each test undertaken in dry

conditions to ensure a uniform relative density across the full channel length. A custom-made load cell, with a maximum load capacity of 1000 N, was used to obtain the reaction force in both vertical and horizontal directions as described in Figure 2. Further information on the load cell arrangement and general equipment set-up can be found in Arnau (2017). The carriage on which all the electronic devices were mounted and to which the iceberg model was attached can travel at different speeds ranging from 0.27 to 0.01 m/s. This range of speeds is very similar to that reported by Smith and Donaldson (1987) on the iceberg drifting speeds. In order to measure the horizontal displacement of the trolley and displacement rate as it moves along the channel, a draw wire sensor was used. All of the instrumentation used were monitored using a USB data acquisition system with data sampling at 0.1 s intervals.

In order to monitor the shearing zones of the sand as the iceberg model is moving, the channel was divided into two parts by means of a plexiglass wall (Figure 3a). Particle Image Velocimetry (PIV) technique was used to study the sand deformation pattern (e.g. Niedostatkiewicz et al., 2011; Leśniewska et al., 2012; Jackson, 2010) and the GeoPIV software (White et al., 2003, Stanier et al., 2016) was employed to perform the PIV analysis. A high-speed digital camera with a resolution of 3648 × 2736 pixels was used in the study and the patch size was set to 40 × 40 pixels, which offered a good compromise between precision and detail (number of measurement points). Depending on the drifting speed of the iceberg model, the camera was set at 10 or 30 fps (frames per second). The number of fps had to be increased as the drifting speed increased in order to keep the search patch small. A camera frame was manufactured to guarantee perpendicularity between the camera (camera lens) and the Plexiglas wall and two halogen lamps were used to guarantee continuous illumination. A constant scale factor of 12.588 pixels/mm was used to transform the displacement field in image-space to object-space. The accuracy associated with this type of transformation was assessed with a chessboard and further information of the experimental set-up can be found in Arnau (2017). For the PIV set-up used in this study, the standard deviation between the true value and the measured quantity was found to be 0.15 mm. This error is in line to that reported by White et al. (2003) in which a constant scale factor and a thick layer of Perspex was used.

| **Parameter** | **This study** | **PRISE study** |
|---|---|---|
| Mean grain size ($D_{50}$) | 0.177 mm | 0.140 mm |
| Effective grain size ($D_{10}$) | 0.126 mm | 0.100 mm |
| Specific gravity | 2.66 | 2.66 |
| Uniformity coefficient | 1.43 | 1.50 |
| Maximum unit weight (γ) | 17.2 kN/m$^3$ | 17.4 kN/m$^3$ |
| Minimum unit weight (γ) | 14.6 kN/m$^3$ | 13.8 KN/m$^3$ |
| Critic friction angle ($\varphi_{critc}$) | 32˚ | 32˚ |
| Peak friction angle ($\varphi_{peak}$) (at prototype scale, $\sigma_n$ = 250 kPa) | 38˚ | 36.5˚ |
| Peak friction angle ($\phi_{peak}$) (at model scale, $\sigma_n$ = 1 kPa) | 48˚ | - |
| $e_{min}$ (min. void ratio) | 0.53 | - |
| $e_{max}$ (max. void ratio) | | - |
| Potential dilation (S) | | - |

| | | |
|---|---|---|
| (at model scale) ($e_0$ = 0.55) | 0.80 | - |
| $E_0$ loose ($\sigma_n$ = 2 kPa, $e_0$ = 0.77) | 0.16 | |
| $E_0$ dense ($\sigma_n$ = 2 kPa, $e_0$ = 0.565 ) | | - |
| $E_0$ loose ($\sigma_n$ = 250 kPa, $e_0$ = 0.77) | 4,500 kPa | - |
| $E_0$ dense ($\sigma_n$ = 250 kPa, $e_0$ = 0.565) | 8,000 kPa | - |
| k loose ($e_0$ = 0.7) | 23,000 kPa | - |
| k dense ($e_0$ = 0.55) | 34,500 kPa | - |
| | $3 \cdot 10^{-4}$ m/s | |
| | $6.2 \cdot 10^{-5}$ m/s | |

**Table 1.** Summary of soil properties

Table 2 presents a summary of the parameters employed during experiments. For example, the range of scour depths that were tested in dry sand and saturated conditions are indicated in Table 2. The iceberg models shown in Figure 4 were used to simulate the scouring process in the laboratory. A total of five different iceberg models were used in this study. Different angles of the frontal face, i.e. the rake angle, were imposed (90°, 120° and 150°) to represent the wide range of shapes of an iceberg keel with a scour width of 150 mm. The smallest iceberg model shown in Figure 4 has a rake angle α = 150°, a scour width of 150 mm and is made of steel. Furthermore, two more iceberg models with a width of 250 mm and 500 mm and a rake angle α = 150° were utilized for this research (see Figure 4). They were made of PVC to make them lighter and easier to handle. It was found that the difference in the construction material had little effect in the resulting scour force as a consequence of the wall-friction angle modification caused by the kinematic wedge (Arnau, 2017). Since the iceberg models tested in the laboratory have walls on the sides (see Figure 2), the frictional effects ($f_s$) on the lateral walls of the model were also studied in order to check if these could have affected the results. A 300x200x1 mm PVC sheet, which minimizes the frontal passive resistance, was dragged along the test bed at a depth of 30 mm and the scour force of 7 N measured. When the side friction $f_s$ and the base friction $f_b$ were compared with the measured scour loads obtained from an iceberg model, it showed an error of less than 5% and hence $f_s$ and $f_b$ were not considered in this study.

**Figure 4. .** Scaled iceberg models with three different scour widths: 150 mm (steel), 250 mm (PVC) and 500 mm (PVC). The rake angle for the three models is α = 150°.

In saturated conditions, the sand bed was prepared using a vibratory probe allowing the preparation of samples at relative densities ranging from 45% to 90% (Arnau, 2017). This allowed the examination of scour tests at different values of sand permeability and dilation potential. In addition, three pore

water pressure transducers PT1, PT2 and PT3 (24 PC series from Honeywell), with a pressure range of 34 kPa, were buried in the sand bed at different depths to capture the pore water pressure reduction near the dilating shear band (see Figure 122). The pressure transducers were positioned at approximately 2.5 m from the starting position of the experiment to allow for a steady state to be achieved. The transducers (PT1, PT2 and PT3) were placed at three different depths to capture the change of pore pressure below the scour depth, see for example Figure 5 where each marker represents a pressure transducer. Based on Figure 5, the pore pressure drop ΔP at the base of the scour (z = 0 m) was calculated assuming that the pore pressure reduces linearly with depth.

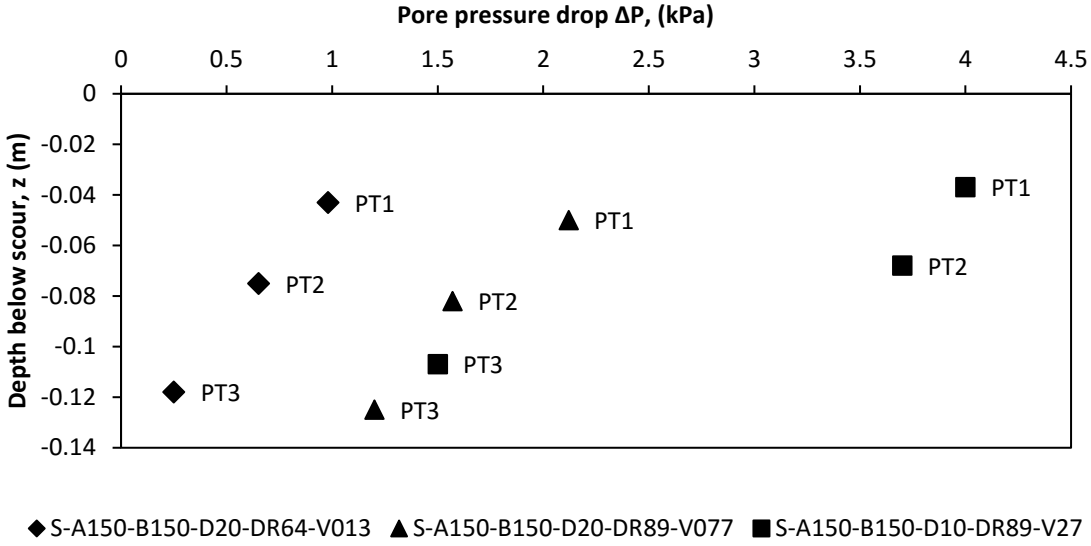


**Figure 5.** Reduction of pore water pressure with depth.

Figure 6 shows how the pore water pressure changed with the position of the iceberg model during a scour test. The plot presented in Figure 6 has been zeroed in order to better reflect the reduction of pore water pressure ΔP. In general, the pore pressure response was characterized by a pronounced reduction as the model ice keel approached the relevant PT followed by a small increase with the passage of the model ice keel over the buried pore pressure transducer. Figure 6 also shows the importance of the position of the transducer, where it can be seen that a larger pressure drop is obtained for transducers closer to the shear band (base of the trench). The data used in Figure 6 corresponds to PT1 and PT2 separated a few millimetres from each other along the sand channel's length.

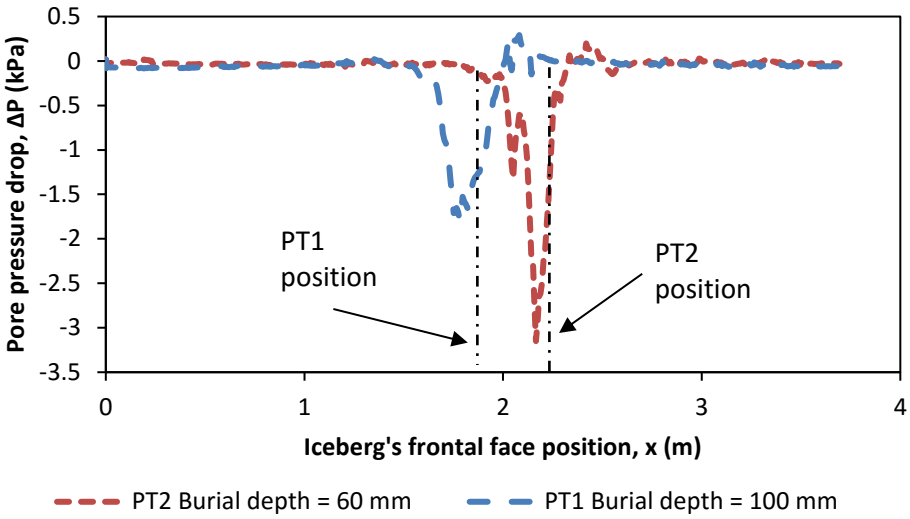


**Figure 6.** Example of the change in pore pressure below the ice model keel at two burial depths.

## Experimental results and observations

Tests are designed to study the significance of different parameters such as, scour depth D, scour width B, rake angle α, drifting speed v and different soil conditions (e.g. initial void ratio, permeability). Table 2 presents a summary of the tests conducted in this study. The test I.D. is constructed as follow: (seabed type)-(rake angle)-(scour width)-(scour depth)-(relative density)-(speed). For example, the test S-A150-B150-D20-DR75-V27 has been conducted in saturated sand at α = 150°, B = 150 mm, D = 20 mm, Dr = 75% and v = 0.27 m/s.

**Table 2.** Summary of tests conducted in this study.

| | | | Dry sand | | Saturated sand | | |
|---|---|---|---|---|---|---|---|
| **Rake angle (α)** | **Scour width B (mm)** | **Construction material** | **Scour depth D (mm)** | **Relative density (%)** | **Scour depth D (mm)** | **Speed v (m/s)** | **Relative density (%)** |
| 150° | 150 | steel | 3 to 45 | 60-75 | 10, 20 and 30 | 0.01 – 0.27 | 45 to 90 |
| | 250 | PVC | 3 to 45 | 60-75 | 10 | 0.01 – 0.21 | 75 to 90 |
| | 500 | PVC | 3 to 45 | 60-75 | 10 | 0.01 – 0.11 | 75 to 90 |
| 120° | 150 | steel | 15 to 45 | 30 - 90 | 10, 20 and 30 | 0.01 – 0.25 | 75 to 90 |
| 90° | 150 | steel | 15 to 45 | 60-75 | 10, 20 and 30 | 0.01 – 0.25 | 45 to 90 |

A typical behaviour of an iceberg scale model scouring the seabed can be described as follow: after the initial contact with the seabed, the forces increase as the sand is accumulated in front of the model. It is assumed that this transient process ends when the amount of sand moved to the sides equals the sand being accumulated in front of the model, after which the force becomes steady and starts to fluctuate as the successive rupture surfaces are formed and overridden by the next rupture

surface. The consequence of this process is best observed in Figure 7. The fluctuating force has a peak that is thought to occur when a new rupture surface is created and is at its full length (see for example Figure 8). The peak load will be described in this paper as $F_{static}$ in the case of dry conditions and $F_{TOT}$ in the case of saturated conditions, where $F_{TOT} = F_{static} + F_{dynamic}$. The peak load is obtained by taking note of all the peak loads registered during a test and calculating the average value. For example, in Figure 7 once the steady state is reached, six peaks were recorded from which the average value was calculated.

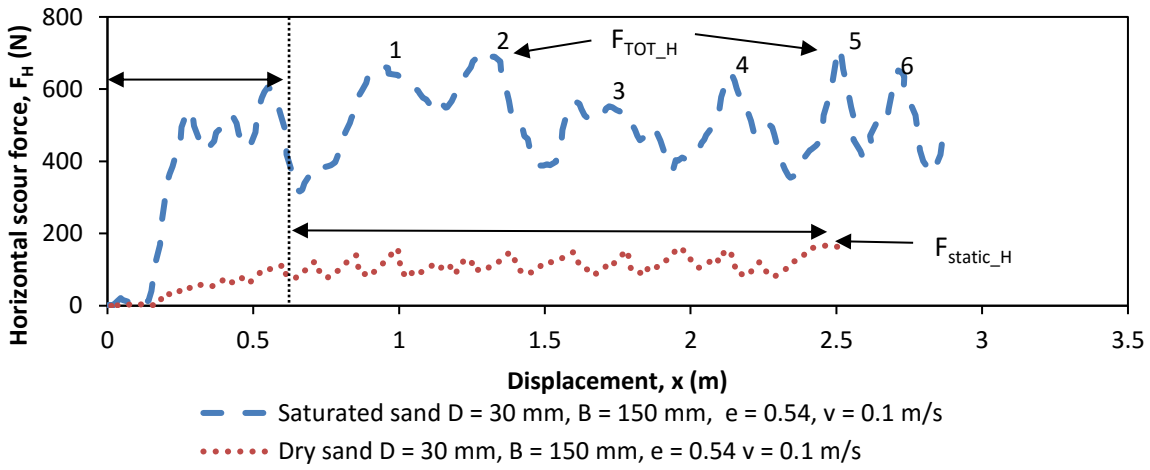


**Figure 7.** Typical scour load fluctuation during a scour test in saturated and dry conditions.

## Stress level and soil failure mechanism

Direct shear box tests were performed at very low effective stresses to provide representative information of the angle of friction developed during the scale model scouring tests under 1g conditions. It is assumed that the mean normal stresses at the shear band for a test in the laboratory are in the range of 1 – 3kPa. Shear box tests undertaken on dry silica sand were carried out for three different relative densities (90% 65% and 5%). As expected, for the samples prepared in dense state, dilation was always present which increased the shear resistance of the samples ($\varphi_p$). The soil friction angle ($\varphi_c$) at critical state was found to be 32°. The dilation angles ($\Psi$) were found to reduce linearly with normal effective stresses on a logarithmic scale, similar to that found by Bolton (1986). For a normal stress of 1kPa a dilation angle, a $\Psi$ of 19° was found, implying a peak friction angle ($\varphi_p$) of 47.2° ($\varphi_p = \varphi_c + 0.8 \cdot \Psi$) during the experiments.

During the plane strain tests in the sand channel, the PIV results indicated a shear plane that originated from the tip of the kinematic wedge and extended to the sand's surface (see Figure 8). This shear plane is inclined at an angle of approximately 21° from the horizontal and formed a sand wedge that can be regarded as a Rankine wedge. The major principal stress in the passive Rankine state is horizontal and shear planes are expected to rise at ($45° - \varphi_p/2$) to the horizontal. This results in an estimated value of the peak friction angle of 48°, which is approximately the same $\varphi_p$ found during the direct shear box tests at low stress levels.

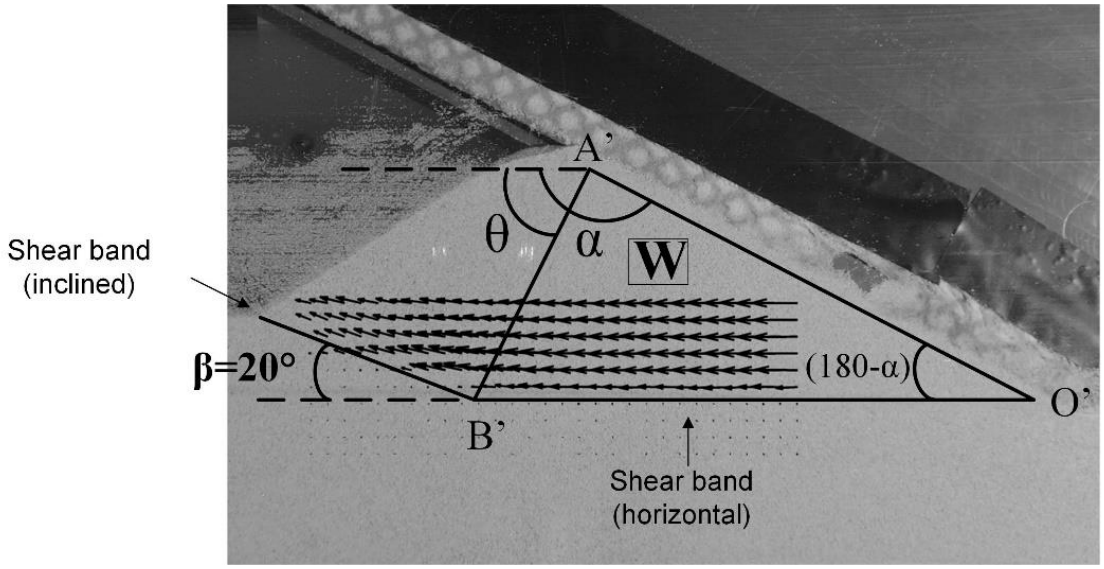


**Figure 8.** PIV displacement field during the plane strain test (D-A150-B150-D20-DR65-V01), where W indicates a kinematic wedge.

## Analytical prediction of ice scour loads in dry sand ($F_{static}$)

Figure 8 and Figure 9 represent the geometry of the soil failure mechanism created in front of an iceberg model with the frontal face inclined at an angle $\alpha = 150^{\circ}$. As can be observed, a kinematic wedge labelled [W] is represented in front of the frontal face of the model. The wall friction angle $\delta$ between the fontal face of the iceberg model (line OA in Figure 9) and the soil cannot be considered to be fully mobilised and its value will remain between $+\delta_{max} < \delta < -\delta_{max}$. As discussed by Arnau and Ivanovic (2015), the wall friction angle $\delta$ was determined experimentally for a range of rake angles with good correlation with the theoretical values proposed by Hettiaratchi and Reece (1975). For the analysis presented herein, the soil-soil interface angle (line A'B' in Figure 9) will be assumed to be $\lambda = \varphi_{crit}$ as suggested by Hettiaratchi and Reece (1975). It was possible to capture the inclination of the shear plane ($\beta$) for three different rake angles $\alpha$ ($90^{o}$, $120^{o}$ and $150^{o}$) during plane strain tests and it was found to be around $21^{o}$ for all three cases. However, it was not possible to capture the soil interface A'B'. There is experimental evidence indicating that $\theta$ matches with the theory of Hettiaratchi and Reece (1975); in Figure 8 an assumed kinematic wedge with an angle $\theta = 90^{\circ}-\varphi_{crit}$ is superimposed on the real shear plane observed under PIV for a rake angle of $150^{o}$. This was repeated for the two other rake angles ($90^{o}$ and $120^{o}$) and the superimposed kinematic wedge with an angle of $\theta = 90^{\circ}-\varphi_{crit}$ matched with the real failure mechanism.

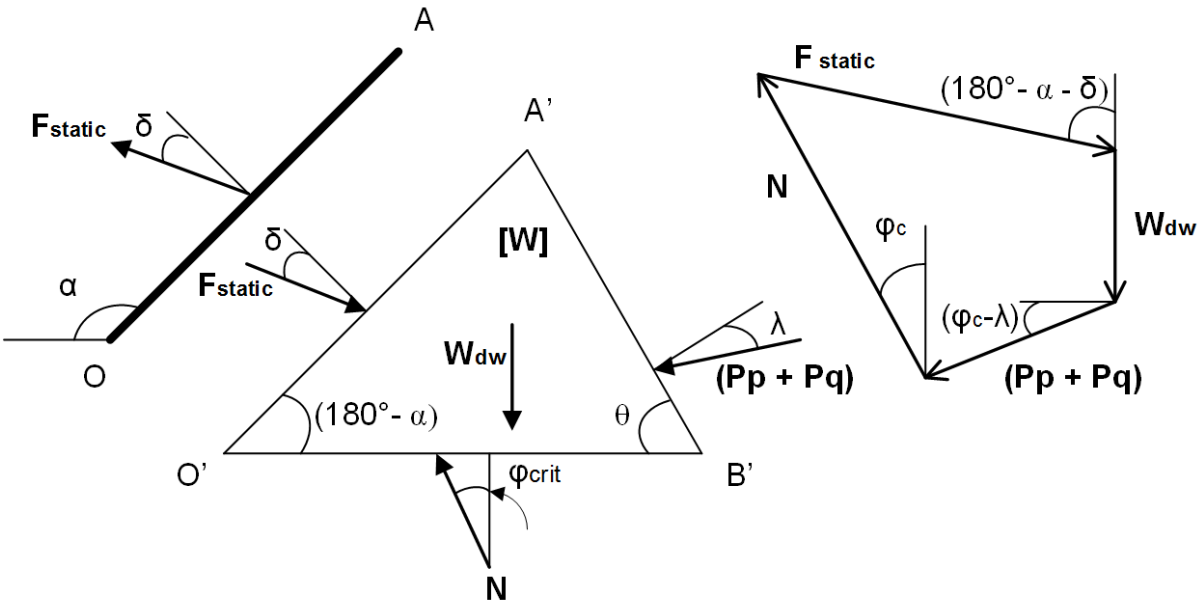


**Figure 9.** Forces acting on the kinematic wedge and force equilibrium diagram during ice scouring in dry conditions.

The polygon of forces acting on the kinematic wedge is obtained with the information described above, which allows the calculation of the reaction force ($F_{static}$) acting on the fontal face of an iceberg (see Figure 9). In addition to the graphical solution, the sum of forces in the horizontal and vertical direction gives that:

$$F_{static} = C_1 \cdot \frac{1}{2}\gamma B(d+D)^2 + C_2(P_p + P_q) \quad (4)$$

where,

$$C_1 = \frac{\tan\varphi_c}{\sin(180-\alpha-\delta)-\tan\varphi_c\cos(180-\alpha-\delta)} \cdot \left(\frac{1}{\tan(180-\alpha)} + \frac{1}{\tan\theta}\right) \quad (5)$$

$$C_2 = \frac{\cos(\varphi_c-\lambda)+\tan\varphi_c\sin(\varphi_c-\lambda)}{\sin(180-\alpha-\delta)-\tan\varphi_c\cos(180-\alpha-\delta)} \quad (6)$$

$P_p = K_P.\gamma \cdot B \cdot D^2$ and $P_q = K_q \cdot q \cdot B \cdot D$, where q is approximated as $q = \gamma_{soil} \cdot d/2$.

The passive earth pressure coefficients $K_P$ and $K_q$ for a rough interface can be calculated using the charts presented by Hettiaratchi and Reece (1974). B is the scour width, d is the height of sand accumulated in front of the iceberg model at the end of each scour test and γ is the soil unit weight. In order to compare the scour loads measured by the load cell with those obtained by Eq. 4, the following adjustments shown in Eq 7 and 8 were required, where δ (Table 3) can adopt positive and negative values (e.g. $+\delta_{max} < \delta < -\delta_{max}$) as discussed in Arnau and Ivanovic (2015).

$$F_{H\_static} = F_{static} \cdot \sin[(180° - \alpha) - \delta] \quad (7)$$

$$F_{V\_static} = F_{static} \cdot \cos[(180° - \alpha) - \delta] \quad (8)$$

Figure 10 shows the height of sand d measured in front of an iceberg model with α = 150°, three different scour widths (150, 250 and 500 mm) and a range of scour depths at the end of each scouring test. The mound height d increases when the scour depth or scour width is increased. Tests conducted at other rake angle (e.g. 90°, 120°) indicated that d increases when α is decreased. It is often assumed that the parameter controlling vertical stresses is the scour depth only, however, Figure 10 indicates that both D and B are important.

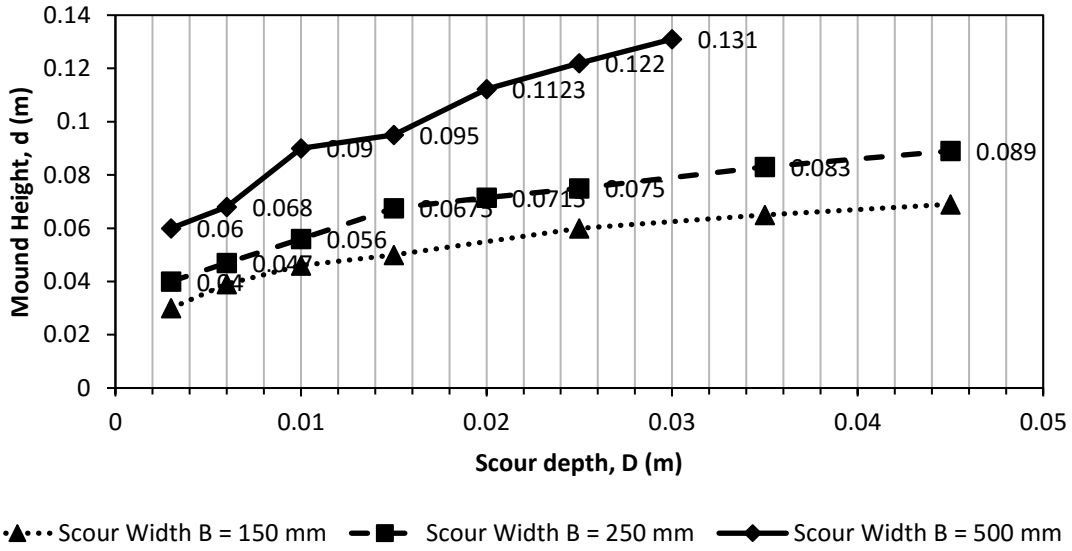


**Figure 10.** Mound height for three different scour widths (150, 250 and 500 mm), rake angle α = 150° and a range of scour depths at $D_r$ = 55-65%.

## Investigation of the rate effects in the presence of kinematic wedges during ice scouring

If two identical scour tests are compared, one with dry sand; the other with saturated sand at a displacement rate that is low enough to generate a fully drained response in the saturated sand, technically, both would be under drained conditions. Figure 11 shows two identical scour test conducted in dry sand and saturated sand. The test in saturated sand is conducted at the lowest possible scouring speed (0.01 m/s) in order to generate a fully drained response in the saturated test bed. As observed, the scour loads from the two tests are almost identical. There is a tacit assumption in this analysis where $F_{TOT} = F_{dynamic} + F_{static}$ and throughout this paper $F_{static}$ can also be referred as $F_{V=0}$ although they are not the exact same thing as discussed later.

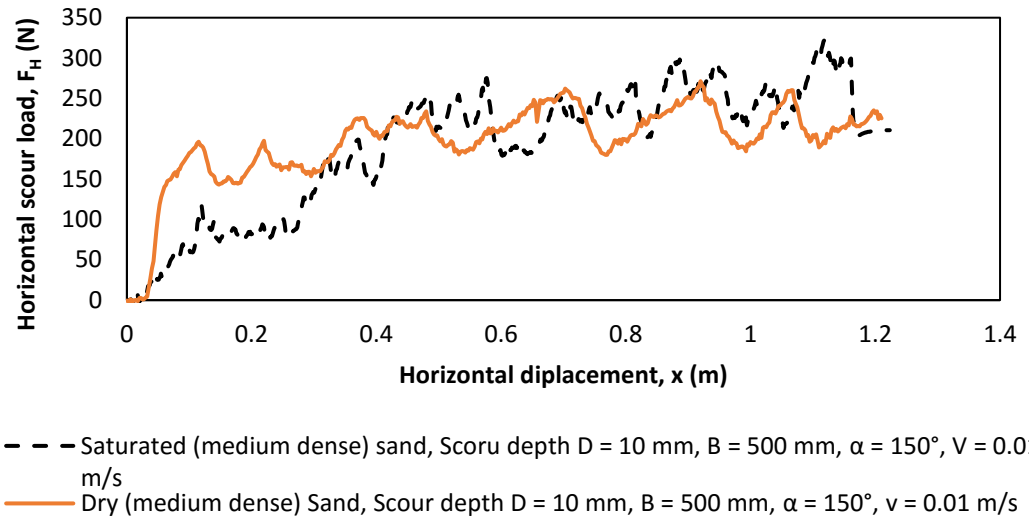


**Figure 11.** Comparison of two identical scour tests in dry sand and saturated sand at a very low displacement rate.

**Pore pressure reduction near the dilating shear band**

The same tests as were carried out in dry conditions were repeated in saturated conditions so that $F_{dynamic}$ and the drop in pore water pressure ΔP could be studied. The rate effects during saturated conditions are caused by a reduction of the pore water pressure within the shear band which causes an increase in the effective stresses. It is assumed that the drop in pore water pressure ΔP will be concentrated mainly in the shear band A and B, as indicated in Figure 12. During the plane strain tests the creation of the successive shear bands occurs and every time a new kinematic wedge is created, pore water will have to flow into the shear band B first and thereafter into shear band A. The changes of the pore pressure were measured with pressure transducers as indicated in Figure 12.

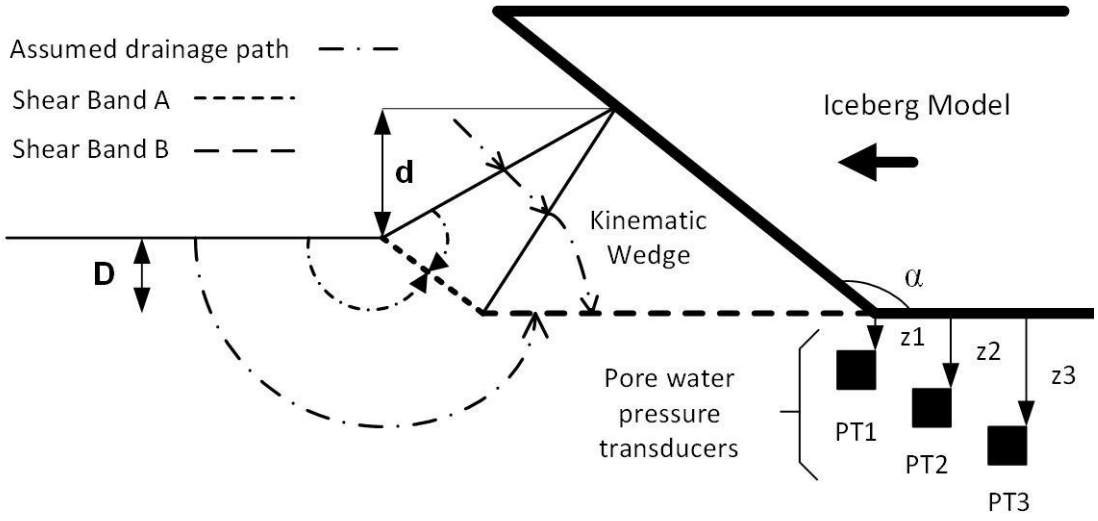


**Figure 12.** Simplification of the assumed drainage paths during ice scouring.

As a general observation, as the rake angle decreases (e.g. from 150° to 90°), the sand accumulated in front of an iceberg model increases and as the scour width increases the frontal mound also increases. As the sand accumulates further in front of the iceberg model and the shear plane B is formed, a larger pressure gradient is required as water will have to flow through a thicker layer of soil and so longer drainage path as indicated in Figure 12. The drop in pore water pressure measured during saturated tests for a range of scour depths and two different rake angles has been represented against $(\gamma vSD/k)$ in Figure 13, where the dilation potential (S) is introduced as suggested by Palmer (1999). Figure 13 shows a common trend line for the tests carried out on models of the same rake angle positioned at different depths. However, when the rake angle decreases from 150$^o$ to 120$^o$ and the height of sand d accumulated in front of the model increases, it produces an increase of the pore pressure drop (solid line in Figure 13). The drop in pore pressure was also found to increase with the scour width.

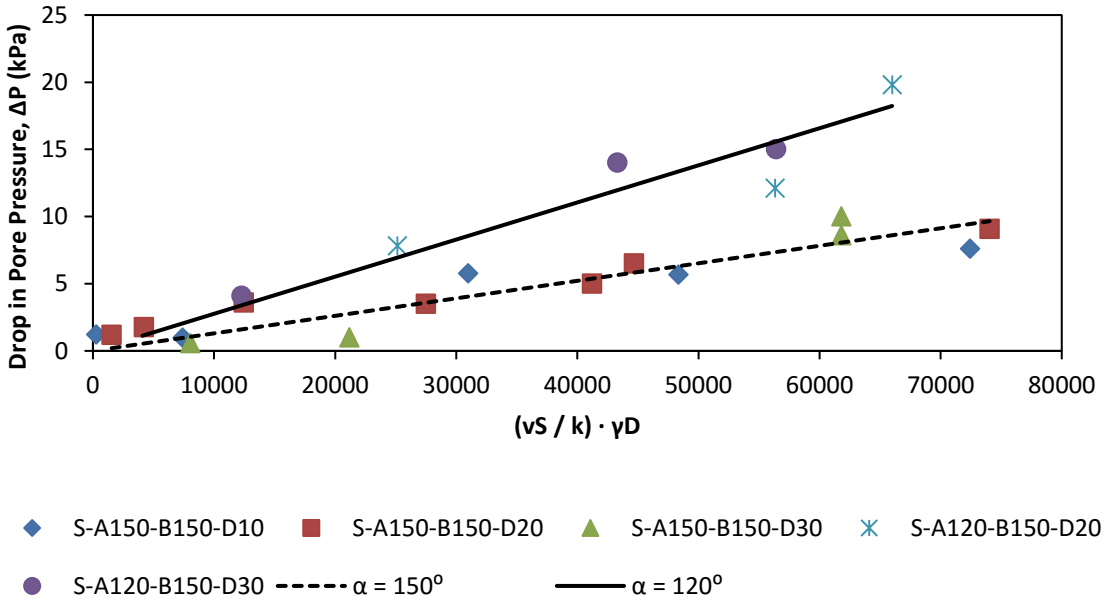


**Figure 13.** Drop in pore water pressure ΔP vs. (vS/k)·γD for three different scour depths D (10 mm, 20 mm and 30 mm) and two rake angles α (150$^o$ and 120$^o$).

Figure 14 contains the same data as Figure 13 but the height of the sand accumulated in front of the model (D+d) has been added on the horizontal axis. The data obtained with a scour width of 250 mm has also been added in the analysis. It can be seen that all the data from the tests undertaken at different scour depths, scour widths and rake angles collapse onto the same trend line. This finding reafirms the assumtion that water has to flow into shear band B, as shown in Figure 12, through a thicker layer of soil.

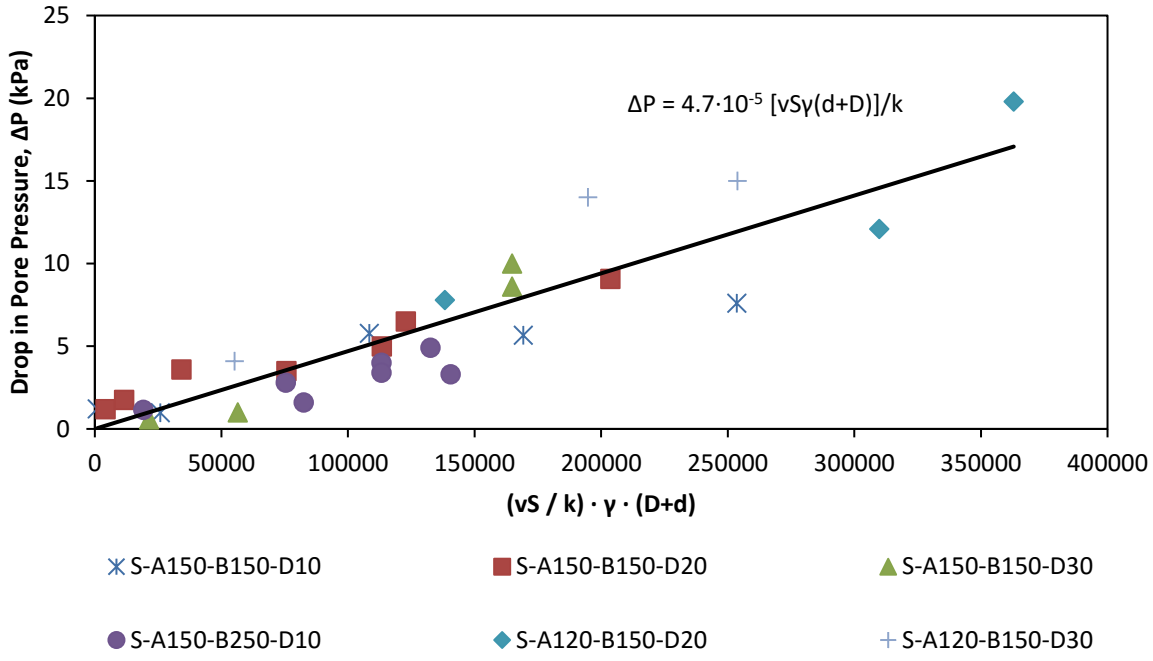


385

386 **Figure 14.** Grouping the drop in pore water pressure in a common trend after introducing the height of sand
387 accumulated in front of the model (d) for different scour depths, scour widths and rake angles.

388 From the analysis shown in Figure 14, Eq. 9 is obtained, which allows the estimation of the pore water
389 pressure drop ΔP during small scale testing in 1g conditions for a range of soil properties and iceberg
390 geometries.

391 $$\Delta P = 4.7 \cdot 10^{-5} \frac{vS}{k} \cdot \gamma_{water} \cdot (D + d) \quad (9)$$

392 Where ΔP is the pore pressure drop in the shear band; v is the drifting speed; S is the dilation potential;
393 $\gamma_{water}$ is the unit weight of water; D is the scour depth; d is the mound height.

394 **Rate effects**

395 Figure 15 to 18 show the influence of the scour depth D, scour width B, drifting speed v, permeability
396 k and initial void ratio $e_0$ on the $F_{TOT}$ and $F_{dynamic}$. The aim is to obtain a general relationship that
397 describes the ice scour loads at different drifting speeds for a range of iceberg geometries and seabed
398 conditions. Figure 15 shows the influence of the scour velocity v (or drifting speed) on the scour load
399 for different scour depths in dense sand ($D_r$ > 75%). Figure 15 shows both the raw experimental data
400 and best straight line fits for each depth. Furthermore, $F_{V=0}$ which is the scour load measured at a
401 velocity near 0 m/s, can be obtained by evaluating the intersection of the trend lines with the vertical
402 axis in Figure 15 and Figure 16. The values of $F_{V=0}$ obtained with this methodology are then used to
403 obtain $F_{dynamic}$ ($F_{dynamic}$ =$F_{TOT}$ - $F_{V=0}$).

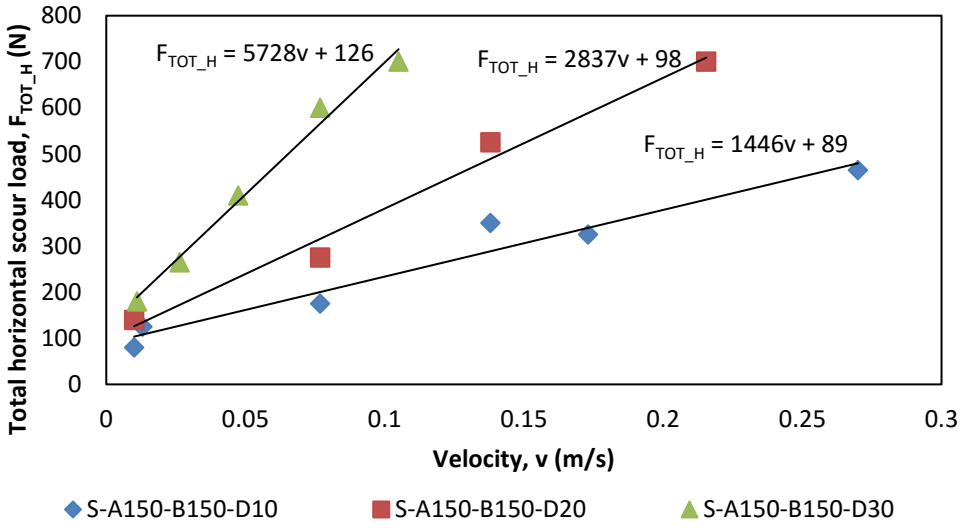


404

405 **Figure 15.** Scour loads ($F_{TOT\_H}$) measured in saturated conditions for a range of towing speeds (v) and
406 scouring depths (D) with fixed scour width B= 150 mm and α = 150° in dense sand ($D_r$ > 75%).

407

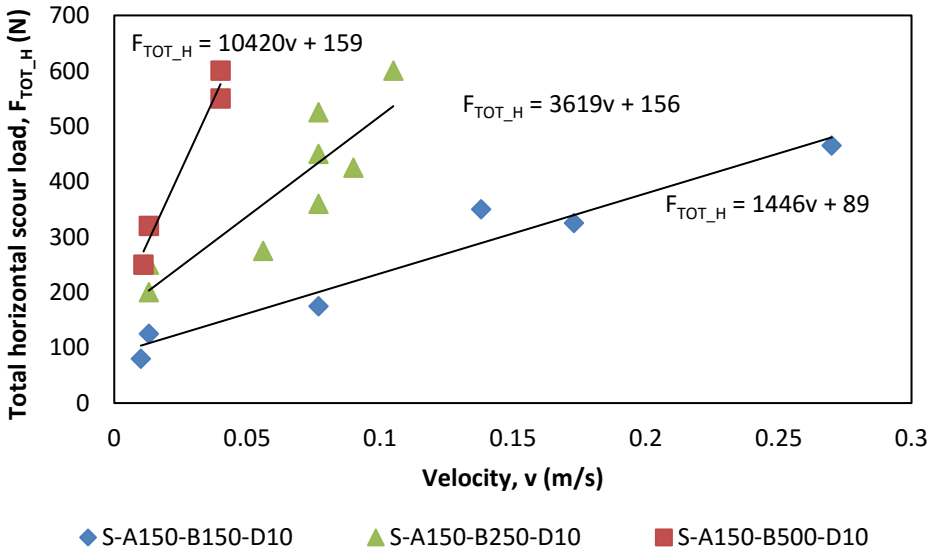


408

409 **Figure 16.** Scour loads ($F_{TOT\_H}$) measured under saturated conditions for a range of towing speeds (v) and
410 scouring widths (150, 250 and 500 mm) with fixed scour depth (10 mm) in dense sand ($D_r$ > 75%).

411

412

413

414

The gradient of the rate effects, dF/dv defined by the trend lines in Figure 15 is presented in Figure 17, which shows that for an iceberg model with an inclined frontal face of α = 150°, the increase in force can be modelled as linear to $(D+d)^2$.

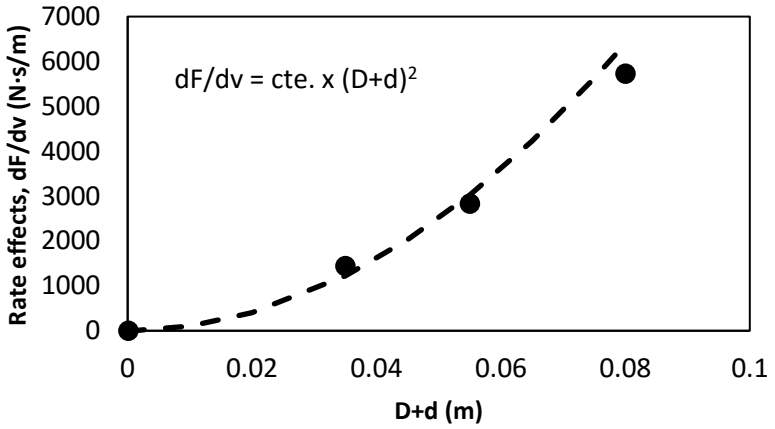


**Figure 17.** Rate effects (dF/dv) vs (D+d) for α = 150˚.

When the same analysis was carried out for the three different scour widths (150, 250 and 500 mm), shown in Figure 16, it was found that the rate effects (dF/dv) increased, with reasonable accuracy, linearly with the scour width B. Equation 1 derived by Barker and Timco (2002) shows that scour loads increased linearly with the scour width too. Furthermore, the present analysis shows that scour loads increased proportional to $(D+d)^2$. The height of sand accumulated in front of the iceberg model was not included in the model presented by Barker and Timco (2002) and for that reason, both models cannot be compared directly. Eq. [1] was derived by (Barker and Timco, 2002) from laboratory studies where two different scour widths of 100 and 200 mm were considered, whereas in this present study three different widths (150, 250 and 500 mm) were used. In order to examine the influence of the differences between the two models, scour loads obtained from Eq. [1] can be compared against the scour loads measured in this present study and also with those obtained from the PRISE studies (shown in the next section).

The usefulness of the analysis shown until this moment is best observed in Figure 18**,** which shows the exact same data as Figure 15 and 16, where, now, the scour loads $F_{Dynamic}$ in the vertical axis were normalized by $B\cdot(D+d)^2$. The data obtained from different soil conditions tested at different scour depths and scour widths collapses into the same trend line in contrast to Figure 15 and 16. The dimensionless group (v/k) was used in the horizontal axis of Error! Reference source not found. to compare tests conducts at different initial soil conditions (e.g. loose and dense state). The same type of analysis was carried out for other rake angles (e.g. 120° and 90°), showing very similar results to those obtained in Figure 18**.**

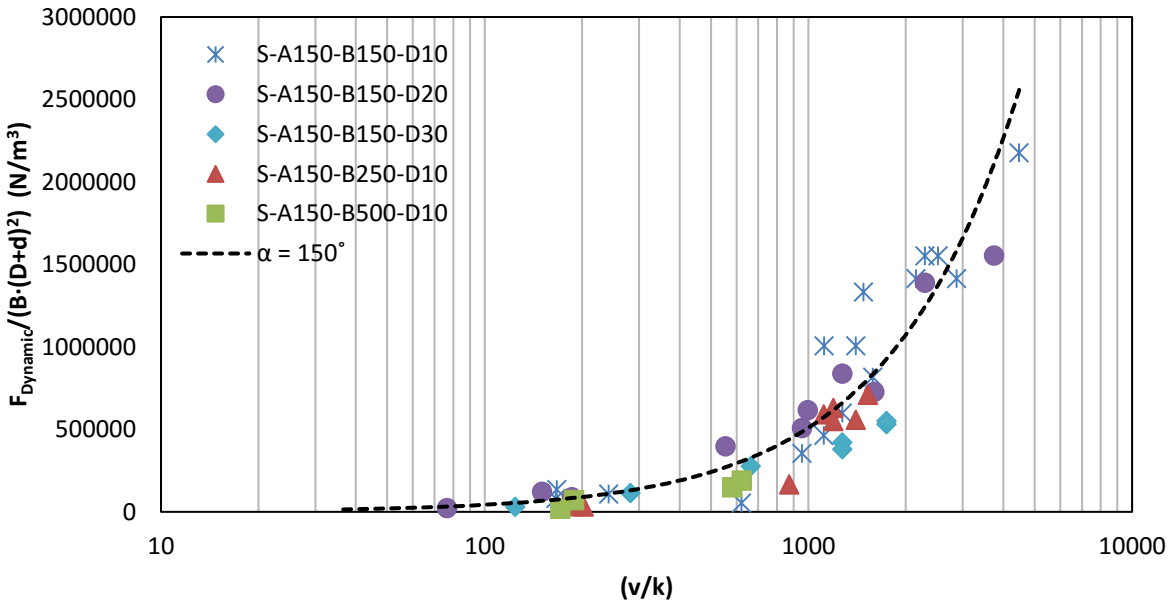


441

442 **Figure 18.** Scour loads $F_{Dynamic}$ normalized by $B\cdot(D+d)^2$ vs. (v/k) in loose and dense sand for D = 10, 20
443 and 30 mm, B = 150, 250 and 500 mm and α = 150˚.

444

445 **Scaled up Forces and Comparison with other experimental results**

446 The forces shown in Figure 18, for example, require the consideration of scale effects of some form.
447 Lauder et al. (2012) and Arnau (2017) showed $e_{crit}$ reducing linearly with normal effective stresses on
448 a logarithmic scale. Lauder et al. (2012) also indicated that the dilation potential S should be
449 determined at the same level of stresses of the prototype, which reduces S at higher stress levels. The
450 soil stiffness modulus $E_o$ (see Table 1) is another parameter that needs to be obtained at the required
451 level of stresses, as previously discussed by Lauder et al. (2012), Lauder and Brown (2014) and Arnau
452 (2017).

453 Lauder and Brown (2014) proposed that the form of rate correction may be more appropriate as
454 multiplicative correction rather than the additive one used in Lauder et al. (2012) and the one used in
455 the previous section, Figure 18. This results in a normalized scour load as indicated in **Error! Reference**
456 **source not found.**, where the scour load normalized by $F_{v=0}$ is plotted against $vS(D+d)/C_V$. This causes
457 the data from tests conducted at different rake angles to collapse onto the same line. Thus, a general
458 relationship that relates the scour force, $F_{TOT\_H}$, with the scour depth D, mound height d, scour width
459 B, scour velocity v, initial void ratio $e_o$, potential dilation S, permeability k and soil stiffness modulus
460 $E_o$ can be found.

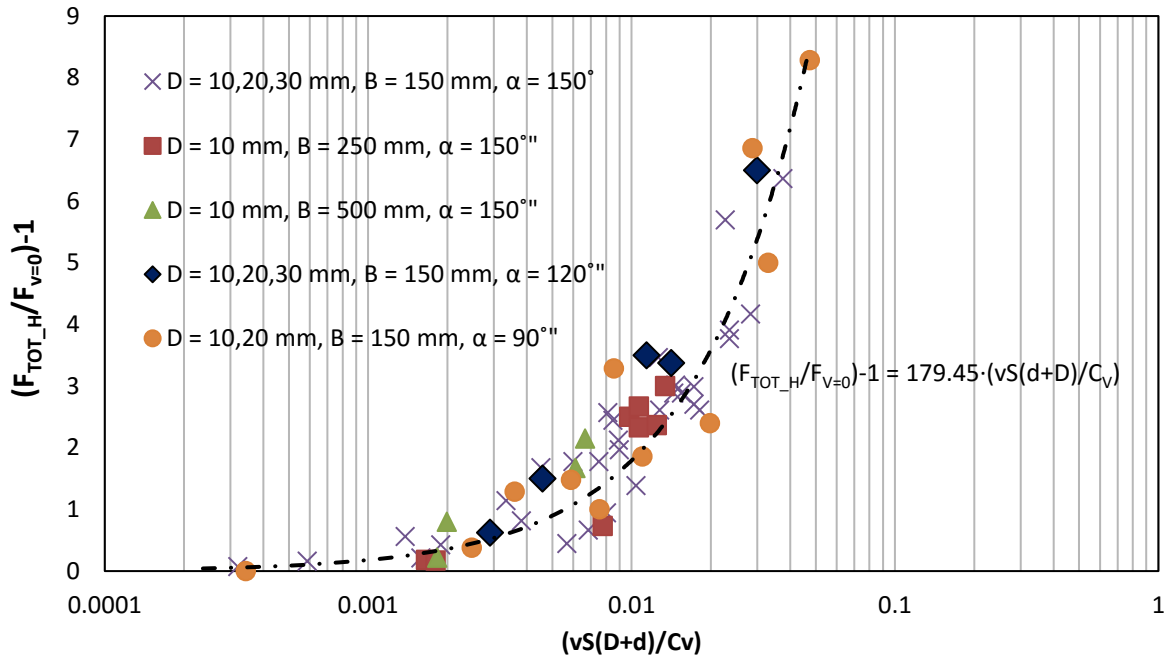


**Figure 19.** Normalized scour force ($F_{TOT\_H}/F_{V=0}$)-1 vs. ($vS(D+d)/C_V$).

The trend line plotted in Figure 19 can be used to predict the total scour loads $F_{TOT\_H}$, which produces an upper bound, and combines the static and dynamic components. This is shown in Eq. 10 and Eq. 7, Eq. 8 and Table 3 can be used to obtain $F_{TOT\_V}$.

$$F_{TOT\_H} = F_{static\_H}\left(179 \cdot \frac{vS(D+d)}{C_V} + 1\right) \qquad \text{Equation 10}$$

Hynes (1996), Winsor and Parson (1997) and Phillips et al. (2005) reported on centrifuge test results in saturated sand undertaken as part of PRISE programme and in particular those related with the scour loads for different ice scour scenarios. Hynes (1996) conducted a total of 8 centrifuge scour tests at a drifting speed of 0.03 m/s. At this drifting speed the rate effects were hardly appreciable. Five of these tests were aimed to simulate a 15 m scour width with a rake angle of 150° and the results are plotted in Figure 20 (triangles). Under these conditions, equation 10 can be used to estimate the scour loads which then can be compared with the results obtained by Hynes (1996). This is shown in **Error! Reference source not found.** by dashed line.

Winsor and Parson (1997) and Phillips et al. (2005) reported 4 more centrifuge scour tests (PRSA01, PRSA03, PRSA04 and PRSA05) at a drifting speed of 0.1 m/s. PRSA01, also plotted in Figure 20 (circle), represent a scour width of 15 m and a rake angle of 150° and is therefore comparable with the centrifuge tests reported by Hynes (1996). Even though PRSA01 was conducted in a sand test bed of high relative density (Dr= 81%) and scour depth of 4.5m, it showed apparent limited rate effects, which is contrary to what was expected. Winsor and Person (1997) reported a limitation of the capacity of the horizontal drive mounted on the centrifuge strongbox which could have been the cause of such low force measured during PRSA01.

PRSA03, PRSA04 and PRSA05 were conducted on a dense sand testbed (e.g. 55 % < $D_r$ < 82%), with a scour width of 15 m, a rake angle of 165° and a drifting speed of 0.1 m/s. The increase of the rake angle, from 150° to 165°, would generally cause 30% increase on the scour loads but not a 60%

485 increase that Figure 20 suggests. Based on the results presented in this paper, the 60 % increase could
486 be caused by the rate effects as the drifting speed was varied from 0.03 m/s to 0.1 m/s. Again, Eq. 10
487 can be used to estimate the scour loads and compare them with the centrifuge results reported by
488 Winsor and Parson (1997) and Phillips et al. (2005). Most of the PRISE centrifuge test results match
489 the scour loads calculated using Eq. 10, which was calibrated from the small scale tests under 1g
490 conditions. Only one test result (PRSA01), marked with a circle in Figure 20 deviates from the trend. It
491 is clear that Eq. 1 derived by Barker and Timco (2002) underestimates the scour loads by one or two
492 orders of magnitude as shown in **Error! Reference source not found.**. The most likely explanation for
493 this disagreement is that the scour loads estimated by Eq. 1 increased proportionally to D, instead of
494 $(D+d)^2$ as it was found in this investigation.

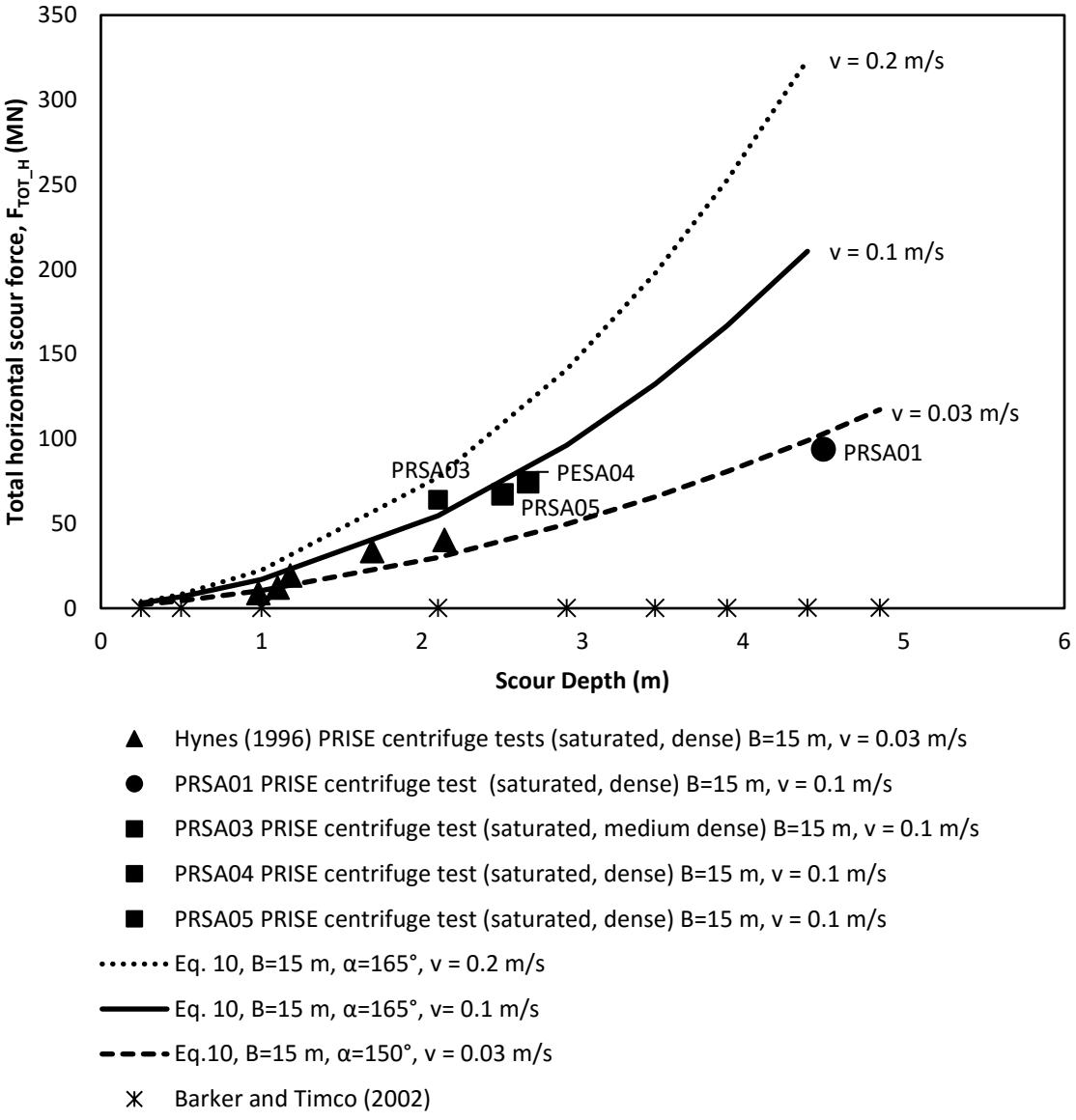

495

496 **Figure 20.** Comparison of measured ice scour loads during PRISE study in a centrifuge and calculated
497 scour loads in saturated conditions in sand at three drifting speeds, 0.03 m/s, 0.1 m/s and 0.2 m/s and
498 a scour widths of 15 m for a range of scouring depths (D).

The soil properties used in Eq. 10 are shown in Table 3. It was found that the soil potential dilation S at prototype scale reduced drastically; for the calculations presented in Figure 20, a potential dilation S = 0.006 was used, which is approximately thirty times smaller than that used during small scale tests in 1g conditions. Such low values of S at prototype scale are in line with the theory of Grinsted (1985), which defines a limit to the increase in the scouring loads with velocity due to the suppression of soil dilation. This limit is reached when the reduction of pore pressure causes an increase of effective stresses to a point which prevents any further soil dilation from occurring, resulting in a potential dilation approaching zero.

**Table 3. Soil conditions used to construct** Error! Reference source not found..

| **Soil Parameter** | **This study (at prototype scale)** |
|---|---|
| Effective grain size ($D_{10}$) | 0.1 mm |
| Submerged weight (γ') | 10.8 KN/m$^3$ |
| $e_o$ | 0.62 (dense) |
| Vertical stress ($\sigma_V$) | 250 KPa (Arnau, 2017) |
| Permeability (k) | 0.0002 (Arnau, 2017) |
| Stiffness modulus ($E_o$) | 35 MPa (Arnau, 2017) |
| Critic friction angle ($\varphi_{critc}$) | 32˚ |
| Peak friction angle ($\varphi_{peak}$) | 38˚ |
| Wall friction angle δ (α = 90°) | 19 ˚ |
| Wall friction angle δ (α = 120°) | -1 ˚ |
| Wall friction angle δ (α = 150°) | -17 ˚ |
| Wall friction angle δ (α = 165°) | -26 ˚ |
| Potential dilation at prototype scale (S) | 0.006 |
| d ( α = 150°) | D(m)=(B^0.9)*0.6*(B/D)^(-0.32) |
| d ( α = 165°) | D(m)=[(B^0.9)*0.6*(B/D)^(-0.32)]*0.75 |
| $K_p$ | 3 |
| $K_q$ | 6.2 |

## Conclusions

Reduced scale models of icebergs were used in a large sand channel with carefully prepared sand beds to investigate the rate effects of an iceberg model scouring a cohesionless seabed at different drifting speeds. Three different rake angles of 150˚, 120˚ and 90˚ and three different scour width of 150 mm, 250 mm and 500 mm were investigated for a range of scour depths and initial soil conditions (e.g. $e_o$, k, $E_o$, $C_v$). The results were compared with existing methods for rate effects evaluation during ploughing and the modifications to these methods have been presented here to describe the rate effects during ice scouring.

It was found that the rate effects increased linearly with $(D+d)^2$ and with the scour width B and **Error! Reference source not found.** is presented as a means to normalize the dynamic component of the scour load ($F_{Dynamic}$). Equally, the pore water pressure drop ΔP increased linearly with (D+d) and eq. 9 represents the change in pore water in the laboratory for a range of initial soil conditions and icebergs geometries.

An empirical relationship, Eq. 10, has been proposed to determine the scour load ($F_{static}$ + $F_{dynamic}$). The rate effects were studied for different soil parameters, which are stress dependent, and also for

524 different scour widths. Thus, Eq. 10 can be used to estimate scouring loads at prototype scale if the
525 one-dimensional stiffness modulus and dilation potential are obtained at the same level of stresses as
526 the prototype. Eq. 1 (Barker and Timco, 2002) was used to compute the scour loads at prototype scale
527 and the computed forces were found to be between one and two orders of magnitude smaller to
528 those obtained in this present study and in PRISE studies. A possible explanation for this disagreement
529 is that the scouring loads obtained from Eq. 1 increase linearly with the scouring width and depth
530 whereas in this present study the scouring loads were found to increase proportionally to $(D+d)^2$.

531 Current models used to predict scour loads in a cohesionless seabed only take into account the static
532 component and assume drained conditions (lower bound). In order to calculate the upper bound, the
533 model described in this paper is proposed, which takes into account the response obtained under
534 undrained (or party-undrained) conditions of a sandy seabed. Figure 20 suggests that an iceberg with
535 a drifting speed of 0.2 m/s can generate scouting loads twice as larger as those reported during PRISE
536 studies.

537 **References**


538 Abdelnour, R. & Graham, B. 1984, "Small scale tests of sea bottom ice scouring", *Proceedings of the*
539 *7th International Symposium on Ice. Association of Hydraulic Engineering and research (IAHR),*
540 Hamburgh, pp. 267-279.

541 Allersma, H.G.B. & Schoonbeek, I.S.S. 2005, "Centrifuge modelling of scouring ice keels in clay",
542 *Proceedings of the 15Th International Offshore and Polar Engineering Conference.* June 19-24,
543 2005, pp. 404-1296.

544 Arnau, S., & Ivanovic, A. 2015. "Predictions of ice scour loads from small scale tests under 1 g
545 conditions", *In Frontiers in Offshore Geotechnics III - 3rd International Symposium on Frontiers*
546 *in Offshore Geotechnics, ISFOG 2015* (pp. 933-938). London: CRC Press/Balkema.

547 Arnau, S. 2017, *Ice gouging in sand and the associated rate effects*, Ph.D Thesis, University of
548 Aberdeen.

549 Barker, A. & Timco, G. 2003, "Laboratory experiments of ice scour processes: buoyant ice
550 model", *Cold Regions Science and Technology,* vol. 36, pp. 103-114.

551 Barker, A. & Timco, G. 2002, "Laboratory experiments of ice scour processes: rigid ice
552 indentor", *Cold Regions Science and Technology,* vol. 35, pp. 195-206.

553 Barrette, P. 2011, "Offshore pipeline protection against seabed gouging by ice: An overview", *Cold*
554 *Regions Science and Technology,* vol. 69, no. 1, pp. 3-20.

555 Barrette, P. & Sudom, D. 2012, "Physical simulations of seabed scouring by ice: Review and
556 database", *Proceedings of the 22Nd International Offshore and Polar Engineering Conference.*
557 *Rhodes, Greece.* June 17-22, pp. 381.

558 Been, K., Croasdale, K., Jordaan, I. & Verlaan, P. 2013, "Practice for pipeline design in ice scoured
559 environments: Application to the Kashagan project", *Proceedings of the 22nd International*
560 *conference on Port and Ocean Engineering under Artic Conditions (POAC), Espoo, Finland.*

561 Been, K., Kosar, K., Hachey, J., Roger, B.T. & Palmer, A.C. 1990, "Ice scour models", *Proceedings*
562 *of the 9th International Conference on Offshore Mechanics and Artic*
563 *Engineering, Houston, Volume 5*, pp. 179.

564 Bolton, M.D. 1986, "The strength and dilatancy of sands", *Geotechnique,* vol. 36, no. 1, pp. 65-78.

565 Campbell, P., Burke, E. & Sonnichsen, G.V. 2014, "Grand Banks Scour Catalogue (GBSC)",
566 *GeoDatabase; Geological Survey of Canada, Open File 7420*.

567 Cathie, D. 2001, "Advances in burial assessment and performance prediction", International cable
568 protection committee plenary meeting. Tokyo, Japan.

569 Cathie, D.N. and Wintgens, J.F. 2001, "Pipeline trenching using plows: Performance and geotechnical
570 hazards", *International Proceedings of the 33rd Annual Offshore Technology Conference (OTC).*
571 *Houston, Texas, 30 April - 3 may.*

572 Croasdale, K., Comfort, G. & Been, K., 2005, "Investigation of ice limits to ice gouging", *Proceedings*
573 *of the 18th International Conference on Port and Ocean Engineering under Artic Conditions*
574 *(POAC), Potsdam*, pp. 23.

575 Eltaher, A. 2014, "Gaps in knowledge and analysis technology of ice-gouge-pipeline
576 interaction", *Proceedings of the Arctic Technology Conference (ATC), Houston, USA, 10-12*
577 *February 2014*.

578 Finnie, I.M.S. 1993, "Performance of shallow foundations in calcareous soils". *Ph.D. thesis*,
579 University of Western Australia, Perth, Australia.

580 Grinsted, T.W. 1985, *Earthmoving in submerged sands, Unpublished Ph.D Thesis*. University of
581 Newcastle upon Tyne

582 Haigh, S.K., Eadington, J. and Madabhushi, S.P.G. 2012, "Permeability and stiffness of sands at very
583 low effective stresses", *Géotechnique,* 62 (1), pp.69-75.

584 Hettiaratchi, D.R.P. & Reece, A.R. 1975, "Boundary wedges in two-dimensional passive soil
585 failure", *Geotechnique,* vol. 25, no. 2, pp. 197-222.

586 Hettiaratchi, D.R.P. & Reece, A.R. 1974, "The calculation of passive soil
587 resistance", *Geotechnique,* vol. 24, no. 3, pp. 289-310.

588 Hynes, F. 1996, *Centrifuge modelling of ice scour in sand*, Master Thesis, Memorial University of
589 Newfoundland.

590 Jackson, P. 2010, *An investigation into the deformation behaviour of geosynthetic reinforced soil*
591 *walls under seismic loading. Master Thesis*, University of Canterbury.

592 King, T. 2011, "Protection of pipelines from ice gouging", *Journal of Pipeline Engineering*, 10(2): 115-
593 120.

594 King, T., Phillips, R., Barrett, J. & Sonnichsen, G. 2009, "Probabilistic pipeline burial analysis for
595 protection against ice scour", *Cold Regions Science and Technology,* vol. 59, no. 1, pp. 58-64.

596 Kioka, S., Yasunaga, Y., Saeki, H. & Nishimakiz, H. 2000, "Evaluation of dominant parameters about
597 the ice scour events", *Proceedings of the 15th International Symposium on Ice Association of*
598 *Hydraulic Engineering and Research (IAHR). Gdańsk, Poland*, pp. 391-401.

599 Lauder, K.D., Brown, M.J., Bransby, M.F. & Gooding, S. 2012, "Variation of tow force with velocity
600 during offshore ploughing in granular materials", *Canadian Geotechnical Journal,* vol. 49, pp.
601 1244-1255.

602 Lauder, K.L. & Brown, M.J. 2014, "Scaling effect in the 1g modelling of offshore pipeline
603 ploughs", *Proceedings of the 8th International Conference on Physical Modelling in Geotechnics.*
604 *Perth, Australia*, 14-17 January, pp. 377-283.

Leśniewska, D., Niedostatkiewicz, M. & Tejchman, J. 2012, "Experimental Study on Shear Localisation in Granular Materials Within Combined Strain and Stress Field", *Strain,* vol. 48, no. 5, pp. 430-444.

Liferov, P., Nes, H., Asklund, J., Shkhinek, K. & Jilenkov, A. 2014, "Ice gouging and its effects on pipelines", *Proceedings of the Arctic Technology Conference (ATC), Houston, USA, 10-12 February.*

Liferov, P. and Høyland, K.V. 2004, "In-situ ice ridge scour tests: experimental set up and basic results", *Cold Regions Science and Technology*, 40 (1-2), pp.97-110.

Niedostatkiewicz, M., Lesniewska, D. & Tejchman, J. 2011, "Experimental analysis of shear zone patterns in cohesionless for earth pressure problems using particle image velocimetry", *Strain,* vol. 47, no. 2, pp. 218-231.

Palmer, A.C. 1999, "Speed effects in cutting and ploughing", *Geotechnique,* vol. 49, no. 3, pp. 285-294.

Paulin, M., Cocker, J., Humby, D. & Lanan, G. 2014, "Trenching of pipelines for protection in ice environments", *Proceedings of the Arctic technology Conference (ATC), Houston USA. 10-12 February.*

Peek, R., Been, K., Bouwman, V., Nobahar, A., Sancio, R. & Schalkwijk, R.V. 2013, "Buried pipeline response to ice gouging on a clay seabed large scale tests and finite elements analysis.", *Proceedings of the 22nd International Conference on Port and Ocean Engineering under Arctic Conditions (POAC), Espoo, Finland.*

Phillips, R. 1995, Centrifuge modelling: Practical considerations. In: R.N. Taylor (Editor), Geotechnical Centrifuge Technology. U.K., London, pp. 34-60.

Phillips, R., Clark, J.I. and Kenny, S. 2005, PRISE studies on gouge forces and subgouge deformations, *Proceedings of the 18$^{Th}$ International Conference on Port and Ocean Engineering Under Arctic Conditions. Vol. 1. Potsdam, USA.* June 26-30, pp. 75-84.

Pike, K. and Kenny, S. 2016, "Offshore pipelines and ice gouge geohazards: comparative performance assessment of decoupled structural and coupled continuum models", *Canadian Geotechnical Journal,* 53 (11), pp.1866-1881.

Smith, S.D. & Donaldson, N.R. 1987, "Dynamic modelling of iceberg drift using current profiles*". Can. Tech. Rep. Hydrogr. Ocean Sci.* No. 91: viii + 125p.

Stanier, S.A., Blaber, J., Take, W.A. & White, D.J. 2016, "Improved image-based deformation measurement for geotechnical applications", *Canadian Geotechnical Journal,* vol. 53, pp. 727-739.

Walter, D.J. & Phillips, R. 1998, *PRISE- Force models for drained and undrained steady state ice scouring*, Contract report, C-Core Publication 98-C33.

White, D.J., Take. W.A. & Bolton, M.D. 2003, "Soil deformation measurement using particle image velocimetry (PIV) and photogrammetry", *Geotechnique,* vol. 53, no. 7, pp. 619-631.

Winsor, R. & Parsons, G. 1997, *Pressure ridge ice scour experiment phase 3c, Extreme ice scour event - Modeling and interpretation, Milestone 2: Centrifuge test PRSA02 data report*, Contract report for BP Alaska, Chevron Petroleum Technology, Exxon Production Research Company, Petro-Canada and Union Texas Petroleum, C-CORE Publication 97-C6.

Woodworth-Lynas, C.M.T., Josenhans, H.W., Barrie, J.V., Lewis, C.F.M. & Parrott, D.R. 1991, "The physical processes of seabed disturbance during iceberg grounding and scouring", *Continental Shelf Research,* vol. 11, no. 8–10, pp. 939-961.

649 Yang, W. 2009, *Physical modeling of subgouge deformations in sand,* Master thesis. Memorial
650 University of Newfoundland.

651
652